Published in final edited form as:
Neuroimage. 2011 June 1; 56(3): 930–938. doi:10.1016/j.neuroimage.2011.02.024.

High-Field (9.4 T) MRI of Brain Dysmyelination by Quantitative Mapping of Magnetic Susceptibility

Chunlei Liu[1,2], **Wei Li**[1], **G. Allan Johnson**[3], and **Bing Wu**[1]

[1]Brain Imaging and Analysis Center, School of Medicine, Duke University, Durham NC

[2]Department of Radiology, School of Medicine, Duke University, Durham NC

[3]Center for In Vivo Microscopy, Department of Radiology School of Medicine, Duke University, Durham NC

Abstract

The multilayered myelin sheath wrapping around nerve axons is essential for proper functioning of the central nervous system. Abnormal myelination leads to a wide range of neurological diseases and developmental disorders. Non-invasive imaging of myelin content is of great clinical importance. The present work demonstrated that loss of myelin in the central nervous system of the shiverer mouse results in a dramatic reduction of magnetic susceptibility in white matter axons. The reduction resulted in a near extinction of susceptibility contrast between gray and white matter. Quantitative magnetic susceptibility imaging and diffusion tensor imaging were conducted on a group of control and shiverer mice at 9.4 T. We measured the resonance frequency distribution of the whole brain for each mouse. Magnetic susceptibility maps were computed and compared between the two groups. It was shown that the susceptibility contrast between gray and white matter was reduced by 96% in the shiverer compared to the controls. Diffusion measurements further confirmed intact fiber pathways in the shiverer mice, ruling out the possibility of axonal injury and its potential contribution to the altered susceptibility. As an autosomal recessive mutation, shiverer is characterized by an almost total lack of central nervous system myelin. Our data provides new evidences indicating that myelin is the predominant source of susceptibility differences between deep gray and white matter observed in magnetic resonance imaging. More importantly, the present study suggests that quantitative magnetic susceptibility is a potential endogenous biomarker for myelination.

Keywords

myelin; magnetic susceptibility imaging; diffusion tensor imaging; MRI

Introduction

Myelin is essential for the proper functioning of the nervous system. Loss of the myelin sheath is the hallmark of a number of neurodegenerative autoimmune diseases (Bitsch et al.,

Correspondence Address: Chunlei Liu, Ph.D. Brain Imaging and Analysis Center Duke University School of Medicine 2424 Erwin Road, Suite 501 Campus Box 2737 Durham, NC 27705 Phone: (919)681 4788 Fax: (919)681 7033 chunlei.liu@duke.edu.

2000; Martin et al., 1992; Timmerman et al., 1992). Early detection of alterations to myelin is critical for early intervention. Unfortunately, quantitative myelin content can only be reliably measured in-vitro, for example, by measuring the myelin basic protein (MBP) with enzyme-linked immunosorbent assay (ELISA) (Nishimura et al., 1986; Spatz et al., 1983), or by myelin staining via immunohistochemical analysis (Hamano et al., 1998). MRI is still the preferred reference test for diagnosing and monitoring the evolution of white-matter development and related diseases due to its excellent soft tissue contrast, high spatial resolution and non-radioactive nature. Commonly used MRI techniques for assessing white matter include, for example, T1, T2-weighted images (Barkovich et al., 1988; Dietrich et al., 1988; Holland et al., 1986), magnetization transfer (Dousset et al., 1992; Henkelman et al., 2001) and diffusion tensor imaging (DTI) (Basser et al., 1994; Moseley et al., 1990).

Recent advances in ultra-high-field (7.0T and above) MRI have opened new venues to study white matter structure and abnormalities (Rauscher et al., 2005). Duyn et al recently reported the observation of subtle layered structure in cortical regions between gray and white matter in high-resolution phase images acquired at 7.0 T (Duyn et al., 2007). The specific source of this contrast is still a topic of research. A number of mechanisms have been suggested including iron stores, proteins and proton exchange (Duyn et al., 2007; Haacke et al., 2007; Shmueli et al., 2009b; Zhong et al., 2008). Although phase images acquired with gradient-echo MRI sequences provide novel tissue contrast, their value for quantitative tissue characterization is limited due to the non-local nature of image phase. The magnetic field at one location that gives rise to the phase is a summation of contributions from all sources surrounding that particular voxel. The strength and orientation of the field is greatly influenced by the position of the subject that can not be easily reproduced. To addressing this issue, there have been growing efforts in developing methods for quantifying the inherent magnetic susceptibility (de Rochefort et al., 2008; de Rochefort et al., 2010; Liu et al., 2009; Shmueli et al., 2009a). These methods have shown promising applications in visualizing tissue structures and in iron quantification (Fukunaga et al., 2010; Haacke et al., 2007; Liu, 2010).

In this study, we report that the absence of myelin in the CNS of the shiverer mouse results in a near disappearance of phase contrast between gray and white matter. Gradient-recalled echo (GRE) images of wild-type and shiverer mouse brains were acquired at 9.4 T. As expected, the phase images of the wild type showed a high contrast between gray and white matter. However, this phase contrast mostly disappeared in the shiverer brains. Quantitative evaluation revealed a 96% reduction of magnetic susceptibility contrast in the white matter. The near disappearance of susceptibility contrast allows a direct visualization of the loss of myelin. DTI experiments were also conducted to verify the axonal integrity and rule out the potential contribution of axonal damages to the observed reduction in susceptibility contrast. We anticipate that quantitative magnetic susceptibility measures may provide a sensitive endogenous marker for myelination.

Methods

Animal model

A number of mutations in mice have been identified that adversely affect oligodendrocyte function and lead to dysmyelination in the CNS. The shiverer mutation is autosomal recessive, characterized by the onset of tremors approximately at the 12^{th} day postnatal, seizures at later times, and a progressive deterioration resulting in an early death (Chernoff, 1981). In this study, three pairs of adult (8 weeks) C3HeB/FeJ control mice and C3FeSWV-Mbp-Shi shiverer mice (The Jackson Laboratory, Bar Harbor, ME) were obtained and anesthetized with Nembutal. To prepare the animal for imaging experiments, a catheter was inserted into the left ventricle of the mouse heart. The animal was perfused with a peristaltic

pump with 20 cc of warm (37°C) 0.9% saline followed by 20 cc of 10% buffered formalin (Buffered Formalde-Fresh; Fisher Scientific) (Johnson et al., 2002). After perfusion fixation, the heads of the mice were stored in 20% buffered formalin overnight before imaging experiments in the following day. The perfused mouse brains were kept within the cranium to prevent any potential damage to the brain caused by surgical removal. To assess the effect of formalin fixative on magnetic susceptibility, two additional pairs of control mice and two additional pairs of shiverer mice were prepared. Specifically, four mice (two controls and two shiverer) were perfused following the aforementioned protocol with a combination of 20 cc saline and 20 cc buffered formalin and were stored in formalin overnight. The other four (two controls and two shiverer) were perfused with 40 cc saline only and were scanned immediately following the perfusion to limit tissue decay. [R2.1] The animal study was approved by the Institutional Animal Care and Use Committee (IACUC) of our institution.

Magnetic resonance imaging protocol

All images were acquired using a 9.4 T (400 MHz) 89-mm vertical bore Oxford magnet with shielded coil providing gradients of 1600 mT/m. The system is controlled by a GE EXCITE MR imaging console, which is nearly identical to those used in the clinical domain. To reduce potential motion during MRI scans, the specimen was positioned tightly inside a cylindrical polyethylene tube (length 30 mm and diameter 11 mm). The tube was filled with Fomblin (perfluoropolyether; Ausimont, Inc., Morristown, NJ) that did not emit proton MR signal thus providing dark background in the image. The tube was sealed with care to avoid air bubbles entering the tube. The use of Fomblin also provided an embedding medium that limits tissue dehydration and susceptibility distortion near the surface of the specimen. Specimens were imaged in a solenoid radiofrequency coil constructed from a single sheet of microwave substrate. The diameter of the solenoid coil was closely matched to the specimen container thus providing high signal sensitivity. The specimens were scanned using a 3D spoiled-gradient-recalled (SPGR) sequence with the following parameters: FOV = $22\times11\times11$ mm^3, matrix = 256×128×128, TE = 28 ms, TR = 50 ms, flip angle = 20° and 2 averages. To generate good phase contrast, TE needs to be sufficiently long. However, longer TE increases T2* decay and consequently decreases signal-to-noise (SNR) ratio. The chosen TE is an experimentally tested tradeoff between tissue contrast and SNR. Longer TR can be used to partially compensate the loss of SNR. The total acquisition time was 27 minutes.

To verify the axonal integrity, diffusion-weighted images were acquired with a 3D spin-echo sequence (Jiang and Johnson, 2010) with the following parameters: FOV = $22\times11\times11$ mm^3, matrix = 164×82×82 (reconstructed to 256x128x128), TE = 12 ms, TR = 2.5s. One image volume was acquired without diffusion weighting. Diffusion weighting was achieved by applying two half-sine gradient pulses around the 180° refocusing pulse. A total of six diffusion encoding directions were used at a b-value of 1500 s/mm^2 to allow the calculation of diffusion tensor. The encoding directions are (1 0 1), (1 0 −1), (1 1 0), (1 −1 0), (0 1 1) and (0, 1 −1). The total scan time was 32.6 hours per specimen. Notice that the non-fixed specimens were not scanned with the DTI protocol due to the possibility of tissue decay. After the MRI experiments, blocks of hippocampal commissure were dissected and stored in fresh fixative overnight at 4°C. Electron microscopy (EM) was taken following standard procedures detailed elsewhere (Harroch et al., 2000; Privat et al., 1979).

MR image analysis

Images were reconstructed with the 3D Fast Fourier Transform (FFT) algorithm on a personal computer equipped with 8 GB RAM and were separated into magnitude and phase. The phase images contain two components: background phase from sources outside the brain (including the receiver coil and, for example, the air-tissue boundaries) and local phase

from tissue susceptibility variation within the brain. The component of interest is the local phase resulting from brain tissue itself. However, the background phase component tends to be much larger than the local tissue phase. As a result, the phase of interest is generally overwhelmed and undistinguishable. Furthermore, the total phase is also typically wrapped. To extract the local phase, we first performed 3D phase unwrapping of the total phase using an algorithm developed by Abdul-Rahman et al (Abdul-Rahman et al., 2007). Since the background phase satisfies Laplacian equation, it can be efficiently removed with a sphere-mean-value (SMV) filter followed by a deconvolution operation (Li and Leigh, 2001; Schweser et al., 2010). The advantage of this SMV filtering method over conventional high-pass filtering method (Haacke et al., 2004; Rauscher et al., 2003) is that the low frequency component of the local phase is also preserved. In the current study, a large filter radius of 9 voxels was employed so that the local phase information is minimally affected during the removal of background phase. The resonance frequency map was calculated from the processed phase image. Quantitative magnetic susceptibility value was computed for each voxel iteratively using the LSQR algorithm (Saunders, 1995) by inverting the following equation (Liu, 2010; Salomir R, 2003):

$$f(\mathbf{r}) = FT^{-1}\left\{\left(\frac{1}{3} - \frac{k_z^2}{k^2}\right)\chi(\mathbf{k})\right\}\gamma H_0 \quad [1]$$

Here, $f(\mathbf{r})$ is the map of frequency offsets; H_0 is the magnitude of the applied magnetic field; $\mathbf{k}$ is the reciprocal space vector and k_z is its z-component; $\chi(\mathbf{k})$ is the Fourier transform of the susceptibility map; γ is gyromagnetic ratio of water proton; FT and FT^{-1} represent Fourier and inverse Fourier transform respectively. In solving Eq. [1], the implementation of the LSQR algorithm by Matlab (MathWorks Inc., Natick, MA) was applied with the default settings (Liu, 2010). Notice that, in this study, both frequency and susceptibility are displayed with a reversed axis following the convention of NMR spectroscopy, i.e. with positive numbers placed on the left side of the axis and negative numbers placed on the right side. As a result, negative values appear bright in the frequency and susceptibility maps while positive values appear dark. DTI images were processed as described previously by calculating the diffusion tensor, eigenvalues, eigenvectors, apparent diffusion coefficient (ADC) and fractional anisotropy (FA) (Basser and Pierpaoli, 1996).

Statistical Analysis

To perform voxel-wise comparison between the control and the shiverer, the brains were coregistered with the nonlinear registration algorithm in FSL (Oxford University, UK). The transformation matrix was optimized based on the registration performed on the magnitude images. It is worth noting that both frequency offsets and susceptibility values measured by MRI are relative quantities. The frequency offset is referenced to the carrier frequency of excitation RF pulses which is determined during the pre-scan. The frequency offset is further affected by the post-processing procedures employed. As a result, the susceptibility values calculated from frequency offsets are also relative values. To make a meaningful comparison and minimize the variations between different scans, we chose to use the adjacent gray matter as an internal reference in comparing the frequency and susceptibility values of the white matter structures between the control and the shiverer mice. Regions-of-interest (ROI) of specific brain structures were manually segmented with the ITK-SNAP software (Yushkevich et al., 2006) using a combination of FA, trace, frequency and magnetic susceptibility maps. The selected ROI were transformed back to the original images. ROIs that clearly exceeded the tissue boundary were revised accordingly and tissue parameters (frequency, susceptibility, FA and trace) were read directly from the original images to avoid interpolation errors. The relative frequency and susceptibility in the selected

structures were computed as the difference between the values in the white matter and the value in the reference ROI.

Results

Loss of susceptibility contrast in dysmyelination

Figure 1A shows a typical phase map computed directly from the complex images. The severe phase wraps completely obscure anatomical structures, for example, the corpus callosum (arrow). Even after unwrapping the phase, the presence of strong background phase overwhelms the tissue structures (Figure 1B). Figure 1C shows the background phase extracted with sphere mean value filtering, illustrating a smooth and unwrapped spatial profile. Figure 1D shows the local phase obtained by subtracting the background phase (Figure 1C) from the total phase (Figure 1B).

Figure 2 compares the phase map, the susceptibility map and the electron micrograph between the control and the shiverer. While the local frequency (Figure 2A) and susceptibility (Figure 2B) of the control mouse demonstrate a high contrast between gray and white matter, such contrast is at a near absence in the shiverer mouse (frequency in Figure 2D and susceptibility in Figure 2E). The electron micrographs reveal thick and dense myelin sheath in the control (Figure 2C) and thin and vanishing myelin sheath in the shiverer (Figure 2F). Figure 3 compares frequency (top row) and susceptibility (bottom row) distributions in selected regions between the control (CTRL) mouse and the shiverer (SHVR) mouse. As illustrated in the histograms, while the mean relative frequency is approximately zero in the shiverer mouse, the mean relative frequency is greater than 2 Hz (absolute value) in the control mouse. On average, the relative frequency changed from −1.22 ~ −3.27 Hz in the control mice to 0.19 ~ 0.34 Hz in the shiverer mice (Table 1). This change resulted in a reduction of frequency contrast by 97% in the corpus callosum and 95% in the hippocampal commissure. Similar to the changes shown in frequency maps, the shiverer mice also exhibited a near extinction of susceptibility contrast between gray and white matter (Figure 3C&D). Specifically, susceptibility contrast is reduced by 98% in the corpus callosum and 95% in the hippocampal commissure. On average, the relative susceptibility values changed from $-1.31 \sim -2.98\times10^{-8}$ in the control mice to $-0.09 \sim 0.04\times10^{-8}$ in the shiverer mice at the corpus callosum, the anterior commissure and the hippocampus (Table 1).

Figure 4 compares the phase and susceptibility contrast of control mice perfused with formalin to those perfused with saline. As shown in this comparison, both methods of perfusion resulted in visually similar tissue contrast. No statistically significant differences were found in the mean susceptibility between these two groups of control mice (corpus callosum: $t = -1.48$, $df = 418$ and $p = 0.14$; hippocampal commissure: $t = 0.74$, $df = 618$ and $p = 0.46$; anterior commissure: $t = -0.009$, $df = 188$ and $p = 0.99$). As expected, neither group of shiverer mice (perfused with formalin and perfused with saline) showed strong contrast between gray and white matter. R2.2

Intact axonal tracts with reduction of diffusion anisotropy and mean diffusivity contrast in dysmyelination

As expected, the shiverer mice displayed similar fiber orientation as the controls (Figure 5A). Figure 5B&C show a decreased FA in the shiverer mouse: a 16% reduction in the corpus callousm and 14% in the hippocampal commissure (Table 1). Although the shift of the histogram in the shiverer mouse is clear, the FA contrast between gray and white matter remains strong. Figure 5D compares the ADC maps between the control and the shiverer. The shiverer mouse exhibits an increased ADC in the white matter which results in a

decrease in the contrast between gray and white matter (Figure 5E&F). The increase in ADC ranges from 6.8% to 27% (Table 1). Specifically, the increase in water diffusivity in the white matter occurs primarily in the two smallest eigenvalues (radial diffusivity) while the largest eigenvalue (axial diffusivity) remains approximately the same (Figure 6). The consistency in radial diffusivity and the unaltered fiber orientation indicate that there is no observable damage to the axon.

Comparison of susceptibility and diffusion contrast

Figure 7 compares the diffusion and susceptibility contrast in three regions of interest: white matter around the ventricles (Figure 7A), the anterior commissure (Figure 7B) and the cerebellum (Figure 7C). Notice that, in the phase maps of the control mice (Figure 7A), the intensity of the corpus callosum (anterior to the ventricles) and the hippocampal commissure (posterior to the ventricles) appears differently with the former appearing dark and the latter appearing bright, even though they have similar magnetic susceptibility. In addition, the spatial extension of the field generated by the CSF blurs the boundary between CSF and brain tissue (solid arrows in Figure 7A). However, the boundary is recovered in the susceptibility maps. Figure 7B shows the contrast in the anterior commissure. Figure 7C demonstrates the change of contrast in the cerebellum. It is interesting to observe that susceptibility provides a far superior delineation of fiber tracts in this region compared to FA (arrows in Figure 7C). In all three regions, quantitative susceptibility maps consistently offer the clearest indication for the loss of myelin in the shiverer mouse.

Table 1 further summarizes the differences in the diffusion and susceptibility measures between the control and the shiverer in a number of representative structures including gray matter, white matter and CSF. As expected, in the gray matter and CSF, both control and shiverer mice have similar FA, ADC and susceptibility values. However, the phase in the CSF varies significantly as a result of the non-localized nature of magnetic dipolar field pattern. As shown in Table 1, although the phase contrast between CSF and gray matter is significantly different between the control and the shiverer mice, the susceptibility contrast is essentially the same ($4.90 \pm 1.33\times10^{-8}$ v.s. $4.34 \pm 1.02\times10^{-8}$). Notice that the large standard deviation in the susceptibility is caused by tissue heterogeneity within the selected ROI rather than by quantification errors. In summary, the reduction in susceptibility contrast in the shiverer mouse is approximately 96% on average. This number roughly agrees with the over 98% reduction of myelin content in adult shiverer mouse (Barbarese et al., 1983).

Discussion

We have demonstrated that, while the phase and susceptibility maps exhibit a strong contrast between gray and white matter in the normal control mouse, this contrast essentially disappears in the myelin-deficient shiverer mouse. Our results indicate that myelin is the primary source of the phase contrast between gray and white matter in the deep brain regions observed at high field strength. More importantly, our findings suggest that the relative susceptibility value between white and gray matter may provide a sensitive endogenous biomarker for myelination.

DTI contrast in the shiverer mouse verifies intact axonal pathways

The primary purpose of the DTI experiments was to quantify the axonal integrity of the white matter pathways and to confirm that any changes observed in the susceptibility contrast are not caused by axonal damages. DTI has been one of the more precise imaging techniques for assessing white matter integrity. It has been routinely reported that diffusion in the white matter becomes increasingly anisotropic as the brain matures which coincides with the natural myelination process (Klingberg et al., 1999; Neil et al., 2002). Based on

animal studies, it is believed that myelin insulates the axons and reduces the radial diffusivity, while having a minimum effect on the axial diffusivity (the largest eigenvalue of the diffusion tensor) (Ono et al., 1995; Song et al., 2002; Tyszka et al., 2006). Our results from DTI experiments are consistent with this general belief. For example, the shiverer mice showed a moderate decrease in FA: 16% in the corpus callousm, 14% in the hippocampal commissure, 1.8% in the anterior commissure and 7% in the hippocampus. These data indicate that myelin may be a significant but not the sole or the primary source of the diffusion anisotropy. The quantification of FA for the hippocamopus may be less accurate compared to other structures due to the smaller size and partial volume effects. On the other hand, diffusivity appears to provide a more sensitive measure to dysmyelination than FA. Despite the increase of ADC, the contrast in the diffusivity remains in the shiverer mice. It is known, however, a reduction in diffusivity is not specific to dysmyelination. Diffusivity and diffusion anisotropy are greatly influenced by many other physiological processes, for example, cell membranes, underlying fiber organizations and extracellular space (Beaulieu, 2002; Neil et al., 2002).

Myelin as the dominant source of susceptibility contrast in deep white matter

The strong phase contrast between gray and white matter has been attributed to a number of potential sources including iron stores (Duyn et al., 2007; Haacke et al., 2007), proteins (Duyn et al., 2007), the proton exchange process between proteins and water molecules (Shmueli et al., 2009b; Zhong et al., 2008) and cylindrical susceptibility inclusion (He and Yablonskiy, 2009). Iron is a known source of strong magnetic susceptibility and there are varying amounts of iron deposited in the brain that are critical for normal brain function. Susceptibility, therefore, has been proposed as a means to quantify iron concentration. However, there has been limited success in quantification of iron content based on susceptibility alone because multiple sources contribute to susceptibility and phase. In a recent study, Fukunaga et al provided strong evidence that iron in ferritin is the dominant source of phase contrast in cortical gray matter, explaining the laminar structures in the cortical layers (Fukunaga et al., 2010). Their data also revealed that some contrast between gray and white matter remains even after iron extraction, suggesting that iron probably is not the main source contrast in deep white matter.

Our data show that, in the absence of myelin, the susceptibility contrast between gray and white matter is nearly extinguished, indicating that this contrast is predominately caused by myelin. Simultaneous DTI studies have ruled out the possibility of axonal damage. From histological studies, it is known that iron concentration in the white matter is similar to that in the gray matter. This knowledge is consistent with our finding that the quantitative susceptibility value of the gray matter does not change significantly in the shiverer mouse. In the white matter, oligodendrocytes are the predominant iron-containing cells. Iron accumulation in the oligodendrocyes is a prerequisite for proper myelination. Nevertheless, studies have shown that iron concentration does not change even in the shiverer mouse (Connor et al., 1993; LeVine, 1991). Their discoveries provide further supporting evidence that myelin is the overwhelming source of the gray and white matter contrast. In addition, myelin is known to be diamagnetic (Lopiano et al., 2000). The loss of myelin in the shiverer mice is therefore expected to cause the white matter to become less diamagnetic. The relative susceptibility of the corpus callosum on average is -1.32×10^{-8} in the control mice and 0.04×10^{-8} in the shiverer which is consistent with the diamagnetic property of myelin. Furthermore, our data also demonstrated that the formalin fixative does not contribute significantly to the strong susceptibility contrast observed in the control mice. Taken together all these evidences, relative susceptibility between white and gray matter appears to be a sensitive marker for myelination.

Interestingly, a very low susceptibility contrast remained at the hippocampal commissure ($-0.46\pm0.79\times10^{-8}$). One possible cause of the remaining contrast can be attributed to residual myelin (Barbarese et al., 1983; Kirschner and Ganser, 1980). Another possible reason could be attributed to larger quantification errors due to its proximity to the CSF which has the largest susceptibility difference comparing to gray matter. Further studies are necessary to understand this small residual contrast. Although our data showed that the formalin fixative does not alter the susceptibility contrast significantly, there was observable inter-subject variability. This variability is likely due to a combination of factors including noise, small sample size and potentially by the orientation dependence of susceptibility. R2.2 One limitation of the current study is that our experimental setup does not allow the characterization of the anisotropic nature of magnetic susceptibility (Lee et al., 2010; Liu, 2010). With the brain placed in a coil perpendicular to the B_0 field, the major fiber bundles are mostly perpendicular to the B_0 field. Further studies are thus necessary to quantify the potential changes in gray and white matter contrast with respect to the B_0-field orientation.

Susceptibility is a more accurate and reliable tissue parameter than phase

The comparative analyses of phase and susceptibility have also demonstrated the advantage of quantitative susceptibility mapping as a more accurate and reliable method for tissue characterization. Although phase (or frequency) maps exhibit strong contrast between gray and white matter, image phase is not an intrinsic property of the brain tissue. The phase value at any given voxel is determined by multiple factors including the local susceptibility, the susceptibility of surrounding voxels, the geometry of the brain structures and the orientation of the brain with respect to the main field. Because of this non-localized property, phase distribution blurs the boundaries of tissue structures further reducing the applicability of phase quantification. For example, the size and shape of the ventricles can significantly alter the phase in the vicinities of the ventricles due to the large susceptibility of the CSF (Figure 7A). As a result, phase cannot be reliably used as a tissue parameter. For example, the frequency of CSF is measured at 0.51 Hz in the control mice but at −1.19 Hz in the shiverer mice even though they have similar susceptibility (Table 1). Susceptibility, on the other hand, is the intrinsic property of the tissue, thus, providing a more meaningful and reliable measure.

One limitation of measuring susceptibility with MRI is its inability to determine the absolute susceptibility. Susceptibility measured with MRI is inherently relative to a predetermined frequency which typically is the carrier frequency of the RF. However, the carrier frequency varies from scan to scan due to differences in field shimming and possible frequency drift. Furthermore, the measured susceptibility is also affected by the background phase removal procedure. If the background phase is removed incorrectly or incompletely, the measured susceptibility will also be inaccurate. This difficulty may be alleviated to a certain degree by placing a reference object with known susceptibility next to the brain. Such requirement is unfortunately undesirable for routine clinical MRI scans. We believe that the use of gray matter as an internal reference offers a viable and convenient alternative. Nevertheless, the reproducibility and the cross-subject variability of the resulting relative susceptibility clearly require more in-depth investigation.

Significance and potential application

Given the critical importance of myelin to normal brain function, we anticipate that mapping magnetic susceptibility may become a useful tool for studying normal brain development and for assessing a wide range of white matter diseases associated with myelin. Myelination is regarded as one of the most useful morphological parameters for evaluating brain development and maturation. Abnormal myelination during brain development can cause a developmental delay, functional disorder, and, in the severe case, premature death (Ono et

al., 1994). In normal brain development, myelination begins early in the 3rd trimester with the most rapid period of myelination occurring in the first two years of life. For example, it occurs early for motor-sensory roots, special senses and the brainstem, while the corticospinal tract starts to myelinate at 36 weeks gestation. By mapping out the changes of magnetic susceptibility along the brain developmental curve, one may thus establish a quantitative relationship between myelin and white matter susceptibility. Such knowledge is invaluable for studying brain development and for diagnosing developmental disorders early.

Imaging susceptibility may also provide a useful prognostic tool for assessing the effectiveness of treatment. There are a large number of neurological diseases caused by abnormalities in the myelin. Research to repair damaged myelin sheaths is ongoing (Archer et al., 1997; Brustle et al., 1999). Techniques include surgically implanting oligodendrocyte precursor cells and Schwann cell precursors in the central nervous system and inducing myelin repair with certain antibodies (Bachelin et al., 2005; Woodhoo et al., 2007). While there have been some encouraging results in mice, it is still unknown whether this technique can be effective in replacing myelin loss in humans (Halfpenny et al., 2002). Quantitative susceptibility mapping may, therefore, provide a critically needed in vivo and non-invasive imaging method to evaluate the treatment outcome.

In conclusion, our study demonstrates that the strong susceptibility contrast observed between gray and white matter nearly vanishes in the absence of myelin. This finding suggests that myelin is likely the predominant cause of the contrast in the deep brain. Our data also demonstrate the advantage of quantitative susceptibility mapping as a more accurate means for characterizing tissue property compared to phase or frequency mapping. Our results further indicate that relative susceptibility between white matter and gray matter may be a useful endogenous biomarker for assessing the intensity of myelination.

Acknowledgments

We are grateful to Laurence Hedlund, Ph.D. and Yi Qi, M.D. for assistance in preparing the specimens. The study is supported by the National Institutes of Health (NIH) through grant R00EB007182 to CL, NCRR National Biomedical Technology Research Center (P41 RR005959 to Duke Center for In Vivo Microscopy) and Small Animal Imaging Resource Program (U24 CA092656) to GAJ.

References

Abdul-Rahman HS, Gdeisat MA, Burton DR, Lalor MJ, Lilley F, Moore CJ. Fast and robust three-dimensional best path phase unwrapping algorithm. Appl Opt. 2007; 46:6623–6635. [PubMed: 17846656]

Archer DR, Cuddon PA, Lipsitz D, Duncan ID. Myelination of the canine central nervous system by glial cell transplantation: a model for repair of human myelin disease. Nat Med. 1997; 3:54–59. [PubMed: 8986741]

Bachelin C, Lachapelle F, Girard C, Moissonnier P, Serguera-Lagache C, Mallet J, Fontaine D, Chojnowski A, Le Guern E, Nait-Oumesmar B, Baron-Van Evercooren A. Efficient myelin repair in the macaque spinal cord by autologous grafts of Schwann cells. Brain. 2005; 128:540–549. [PubMed: 15689363]

Barbarese E, Nielson ML, Carson JH. The effect of the shiverer mutation on myelin basic protein expression in homozygous and heterozygous mouse brain. J Neurochem. 1983; 40:1680–1686. [PubMed: 6189969]

Barkovich AJ, Kjos BO, Jackson DE Jr. Norman D. Normal maturation of the neonatal and infant brain: MR imaging at 1.5 T. Radiology. 1988; 166:173–180. [PubMed: 3336675]

Basser PJ, Mattiello J, LeBihan D. Estimation of the effective self-diffusion tensor from the NMR spin echo. J Magn Reson B. 1994; 103:247–254. [PubMed: 8019776]

Basser PJ, Pierpaoli C. Microstructural and physiological features of tissues elucidated by quantitative-diffusion-tensor MRI. J Magn Reson B. 1996; 111:209–219. [PubMed: 8661285]

Beaulieu C. The basis of anisotropic water diffusion in the nervous system - a technical review. NMR Biomed. 2002; 15:435–455. [PubMed: 12489094]

Bitsch A, Schuchardt J, Bunkowski S, Kuhlmann T, Bruck W. Acute axonal injury in multiple sclerosis. Correlation with demyelination and inflammation. Brain. 2000; 123(Pt 6):1174–1183. [PubMed: 10825356]

Brustle O, Jones KN, Learish RD, Karram K, Choudhary K, Wiestler OD, Duncan ID, McKay RD. Embryonic stem cell-derived glial precursors: a source of myelinating transplants. Science. 1999; 285:754–756. [PubMed: 10427001]

Chernoff GF. Shiverer: an autosomal recessive mutant mouse with myelin deficiency. J Hered. 1981; 72:128. [PubMed: 6168677]

Connor JR, Roskams AJ, Menzies SL, Williams ME. Transferrin in the central nervous system of the shiverer mouse myelin mutant. J Neurosci Res. 1993; 36:501–507. [PubMed: 7511695]

de Rochefort L, Brown R, Prince MR, Wang Y. Quantitative MR susceptibility mapping using piece-wise constant regularized inversion of the magnetic field. Magn Reson Med. 2008; 60:1003–1009. [PubMed: 18816834]

de Rochefort L, Liu T, Kressler B, Liu J, Spincemaille P, Lebon V, Wu J, Wang Y. Quantitative susceptibility map reconstruction from MR phase data using bayesian regularization: validation and application to brain imaging. Magn Reson Med. 2010; 63:194–206. [PubMed: 19953507]

Dietrich RB, Bradley WG, Zaragoza E.J.t. Otto RJ, Taira RK, Wilson GH, Kangarloo H. MR evaluation of early myelination patterns in normal and developmentally delayed infants. AJR Am J Roentgenol. 1988; 150:889–896. [PubMed: 2450448]

Dousset V, Grossman RI, Ramer KN, Schnall MD, Young LH, Gonzalez-Scarano F, Lavi E, Cohen JA. Experimental allergic encephalomyelitis and multiple sclerosis: lesion characterization with magnetization transfer imaging. Radiology. 1992; 182:483–491. [PubMed: 1732968]

Duyn JH, van Gelderen P, Li TQ, de Zwart JA, Koretsky AP, Fukunaga M. High-field MRI of brain cortical substructure based on signal phase. Proc Natl Acad Sci U S A. 2007; 104:11796–11801. [PubMed: 17586684]

Fukunaga M, Li TQ, van Gelderen P, de Zwart JA, Shmueli K, Yao B, Lee J, Maric D, Aronova MA, Zhang G, Leapman RD, Schenck JF, Merkle H, Duyn JH. Layer-specific variation of iron content in cerebral cortex as a source of MRI contrast. Proc Natl Acad Sci U S A. 2010; 107:3834–3839. [PubMed: 20133720]

Haacke EM, Ayaz M, Khan A, Manova ES, Krishnamurthy B, Gollapalli L, Ciulla C, Kim I, Petersen F, Kirsch W. Establishing a baseline phase behavior in magnetic resonance imaging to determine normal vs. abnormal iron content in the brain. J Magn Reson Imaging. 2007; 26:256–264. [PubMed: 17654738]

Haacke EM, Xu Y, Cheng YC, Reichenbach JR. Susceptibility weighted imaging (SWI). Magn Reson Med. 2004; 52:612–618. [PubMed: 15334582]

Halfpenny C, Benn T, Scolding N. Cell transplantation, myelin repair, and multiple sclerosis. Lancet Neurol. 2002; 1:31–40. [PubMed: 12849543]

Hamano K, Takeya T, Iwasaki N, Nakayama J, Ohto T, Okada Y. A quantitative study of the progress of myelination in the rat central nervous system, using the immunohistochemical method for proteolipid protein. Brain Res Dev Brain Res. 1998; 108:287–293.

Harroch S, Palmeri M, Rosenbluth J, Custer A, Okigaki M, Shrager P, Blum M, Buxbaum JD, Schlessinger J. No obvious abnormality in mice deficient in receptor protein tyrosine phosphatase beta. Mol Cell Biol. 2000; 20:7706–7715. [PubMed: 11003666]

He X, Yablonskiy DA. Biophysical mechanisms of phase contrast in gradient echo MRI. Proc Natl Acad Sci U S A. 2009; 106:13558–13563. [PubMed: 19628691]

Henkelman RM, Stanisz GJ, Graham SJ. Magnetization transfer in MRI: a review. NMR Biomed. 2001; 14:57–64. [PubMed: 11320533]

Holland BA, Haas DK, Norman D, Brant-Zawadzki M, Newton TH. MRI of normal brain maturation. AJNR Am J Neuroradiol. 1986; 7:201–208. [PubMed: 3082150]

Jiang Y, Johnson GA. Microscopic diffusion tensor imaging of the mouse brain. Neuroimage. 2010; 50:465–471. [PubMed: 20034583]

Johnson GA, Cofer GP, Gewalt SL, Hedlund LW. Morphologic phenotyping with MR microscopy: the visible mouse. Radiology. 2002; 222:789–793. [PubMed: 11867802]

Kirschner DA, Ganser AL. Compact myelin exists in the absence of basic protein in the shiverer mutant mouse. Nature. 1980; 283:207–210. [PubMed: 6153124]

Klingberg T, Vaidya CJ, Gabrieli JD, Moseley ME, Hedehus M. Myelination and organization of the frontal white matter in children: a diffusion tensor MRI study. Neuroreport. 1999; 10:2817–2821. [PubMed: 10511446]

Lee J, Shmueli K, Fukunaga M, van Gelderen P, Merkle H, Silva AC, Duyn JH. Sensitivity of MRI resonance frequency to the orientation of brain tissue microstructure. Proc Natl Acad Sci U S A. 2010; 107:5130–5135. [PubMed: 20202922]

LeVine SM. Oligodendrocytes and myelin sheaths in normal, quaking and shiverer brains are enriched in iron. J Neurosci Res. 1991; 29:413–419. [PubMed: 1920537]

Li L, Leigh JS. High-precision mapping of the magnetic field utilizing the harmonic function mean value property. J Magn Reson. 2001; 148:442–448. [PubMed: 11237651]

Liu C. Susceptibility tensor imaging. Magn Reson Med. 2010; 63:1471–1477. [PubMed: 20512849]

Liu T, Spincemaille P, de Rochefort L, Kressler B, Wang Y. Calculation of susceptibility through multiple orientation sampling (COSMOS): a method for conditioning the inverse problem from measured magnetic field map to susceptibility source image in MRI. Magn Reson Med. 2009; 61:196–204. [PubMed: 19097205]

Lopiano L, Fasano M, Giraudo S, Digilio G, Koenig SH, Torre E, Bergamasco B, Aime S. Nuclear magnetic relaxation dispersion profiles of substantia nigra pars compacta in Parkinson's disease patients are consistent with protein aggregation. Neurochem Int. 2000; 37:331–336. [PubMed: 10825573]

Martin R, McFarland HF, McFarlin DE. Immunological aspects of demyelinating diseases. Annu Rev Immunol. 1992; 10:153–187. [PubMed: 1375472]

Moseley ME, Cohen Y, Kucharczyk J, Mintorovitch J, Asgari HS, Wendland MF, Tsuruda J, Norman D. Diffusion-weighted MR imaging of anisotropic water diffusion in cat central nervous system. Radiology. 1990; 176:439–445. [PubMed: 2367658]

Neil J, Miller J, Mukherjee P, Huppi PS. Diffusion tensor imaging of normal and injured developing human brain - a technical review. NMR Biomed. 2002; 15:543–552. [PubMed: 12489100]

Nishimura RN, Wang J, Merrill JE, Mickey MR, Myers LW. Quantitation of myelination and demyelination by the measurement of myelin basic protein by ELISA. J Neurol Sci. 1986; 73:317–324. [PubMed: 2425056]

Ono J, Harada K, Takahashi M, Maeda M, Ikenaka K, Sakurai K, Sakai N, Kagawa T, Fritz-Zieroth B, Nagai T, et al. Differentiation between dysmyelination and demyelination using magnetic resonance diffusional anisotropy. Brain Res. 1995; 671:141–148. [PubMed: 7728526]

Ono J, Harada K, Yamamoto T, Onoe S, Okada S. Delayed myelination in a patient with 18q- syndrome. Pediatr Neurol. 1994; 11:64–67. [PubMed: 7527214]

Privat A, Jacque C, Bourre JM, Dupouey P, Baumann N. Absence of the major dense line in myelin of the mutant mouse "shiverer". Neurosci Lett. 1979; 12:107–112. [PubMed: 460693]

Rauscher A, Barth M, Reichenbach JR, Stollberger R, Moser E. Automated unwrapping of MR phase images applied to BOLD MR-venography at 3 Tesla. J Magn Reson Imaging. 2003; 18:175–180. [PubMed: 12884329]

Rauscher A, Sedlacik J, Barth M, Mentzel HJ, Reichenbach JR. Magnetic susceptibility-weighted MR phase imaging of the human brain. AJNR Am J Neuroradiol. 2005; 26:736–742. [PubMed: 15814914]

Salomir R DSB, Moonen CTW. A fast calculation method for magnetic field inhomogeneity due to an arbitrary distribution of bulk susceptibility. Concepts in Magnetic Resonance Part B. 2003; 19B: 26–34.

Saunders M. Solution of sparse rectangular systems using LSQR and CRAIG. BIT Numerical Mathematics. 1995; 35:588–604.

Schweser, F.; Lehr, BW.; Deistung, A.; Reichenbach, JR. A novel approach for separation of background phase in SWI phase data utilizing the harmonic function mean value propert. Proc of International Society of Magnetic Resonance in Medicine; Stockholm, Sweden. 2010. p. 142

Shmueli K, de Zwart JA, van Gelderen P, Li TQ, Dodd SJ, Duyn JH. Magnetic susceptibility mapping of brain tissue in vivo using MRI phase data. Magn Reson Med. 2009a; 62:1510–1522. [PubMed: 19859937]

Shmueli K, Li T-Q, Yao B, Fukunaga M, Duyn JH. The contribution of exchange to MRI phase contrast in the human brain. Neuroimage. 2009b; 47:S72.

Song SK, Sun SW, Ramsbottom MJ, Chang C, Russell J, Cross AH. Dysmyelination revealed through MRI as increased radial (but unchanged axial) diffusion of water. Neuroimage. 2002; 17:1429–1436. [PubMed: 12414282]

Spatz L, Whitman L, Messito MJ, Nilaver G, Ginsberg S, Latov N. Measurement of myelin basic protein and of anti-basic protein antibodies by ELISA utilizing biotinylated antibodies. Immunol Commun. 1983; 12:31–37. [PubMed: 6194103]

Timmerman V, Nelis E, Van Hul W, Nieuwenhuijsen BW, Chen KL, Wang S, Ben Othman K, Cullen B, Leach RJ, Hanemann CO, et al. The peripheral myelin protein gene PMP-22 is contained within the Charcot-Marie-Tooth disease type 1A duplication. Nat Genet. 1992; 1:171–175. [PubMed: 1303230]

Tyszka JM, Readhead C, Bearer EL, Pautler RG, Jacobs RE. Statistical diffusion tensor histology reveals regional dysmyelination effects in the shiverer mouse mutant. Neuroimage. 2006; 29:1058–1065. [PubMed: 16213163]

Woodhoo A, Sahni V, Gilson J, Setzu A, Franklin RJ, Blakemore WF, Mirsky R, Jessen KR. Schwann cell precursors: a favourable cell for myelin repair in the Central Nervous System. Brain. 2007; 130:2175–2185. [PubMed: 17550908]

Yushkevich PA, Piven J, Hazlett HC, Smith RG, Ho S, Gee JC, Gerig G. User-guided 3D active contour segmentation of anatomical structures: significantly improved efficiency and reliability. Neuroimage. 2006; 31:1116–1128. [PubMed: 16545965]

Zhong K, Leupold J, von Elverfeldt D, Speck O. The molecular basis for gray and white matter contrast in phase imaging. Neuroimage. 2008; 40:1561–1566. [PubMed: 18353683]

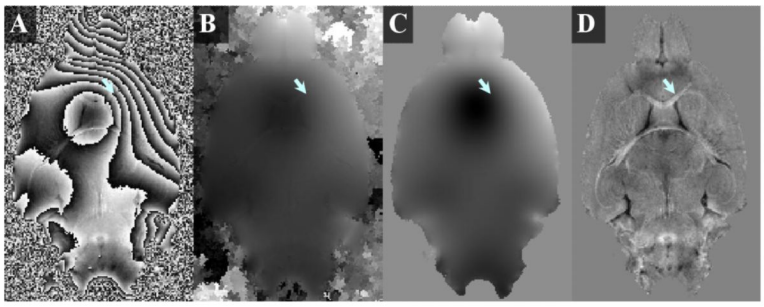

Figure 1.

Illustration of the processing of phase images. (A) A representative example of raw phase map calculated directly from the complex image contains strong background phase and severe phase wrapping. (B) The corresponding phase map after unwrapping with ITK-SNAP. Tissue contrast is overwhelmed by strong background phase. (C) The background phase map extracted with the sphere mean method. (D) The local phase map after background phase removal reveals high contrast (arrow).

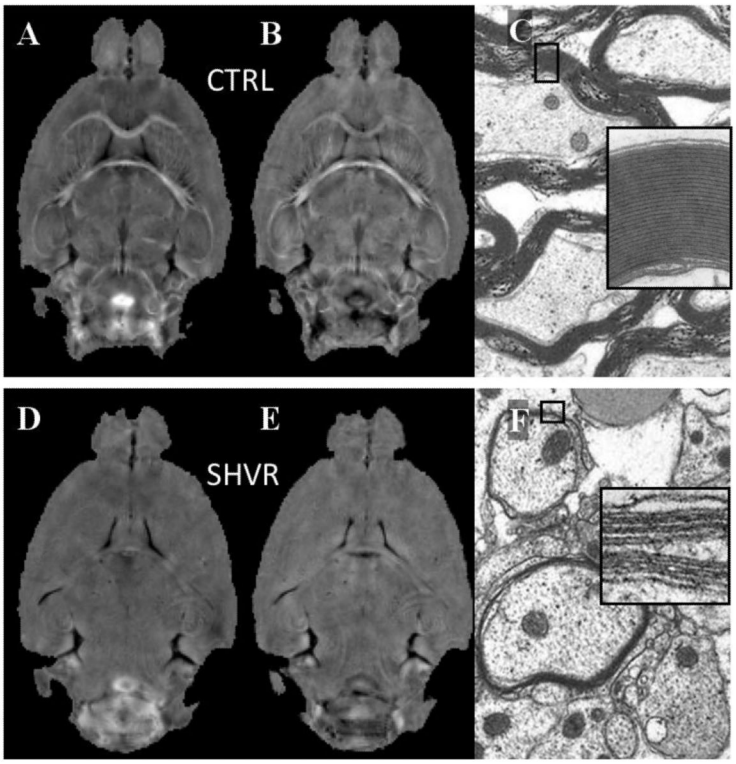

Figure 2.

Loss of frequency and susceptibility contrast in the shiverer mice. The top row shows images of control (CTRL) mice and the bottom row shows shiverer (SHVR) mice. (A) A representative frequency map of the control mouse demonstrates high contrast between gray and white matter. (B) Corresponding susceptibility map also shows high contrast. (C) Electron micrograph of the control mouse shows myelinated axons with thick and dense myelin sheath (inset shows an enlarged view of a selected myelin sheath). (D) The frequency map at the same slice of the shiverer mouse reveals a near absence of gray-white matter contrast. (E) Corresponding susceptibility map. (F) Electron micrograph of hippocampal commissure$^{R2.3}$ reveals dysmyelination in shiverer mice (inset shows few lamellas in the myelin sheath).

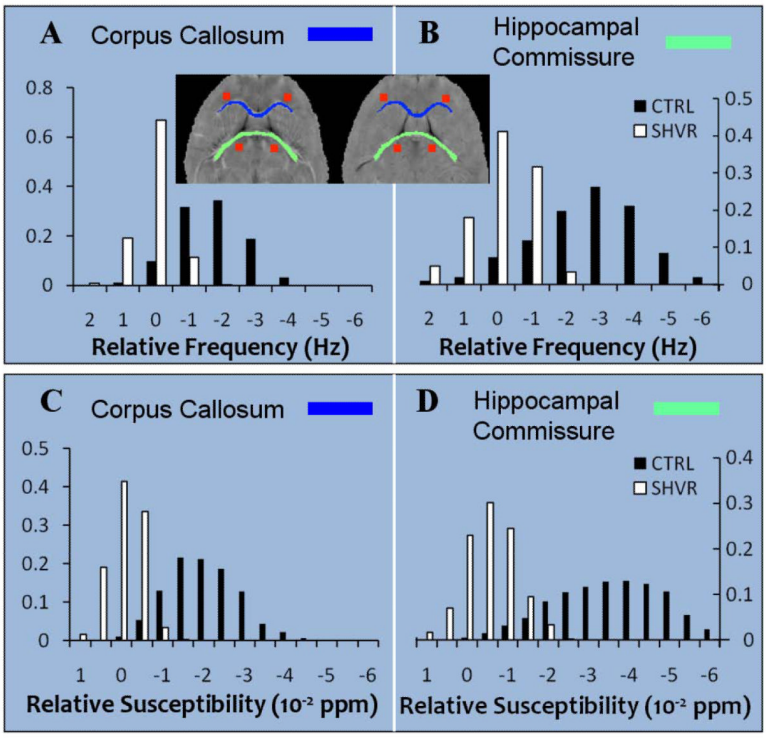

Figure 3.

Quantitative comparison of phase and susceptibility contrast in the control and the shiverer mice. (A) Comparison of the histograms of relative frequency in the corpus callosum between the control and the shiverer and (B) comparison of the frequency histogram in the hippocampal commissure demonstrate a loss of tissue contrast in the shiverer mice. Inset shows the ROIs in the control (left) and the shiverer (right) mouse: corpus callosum (blue) and the corresponding reference ROI (orange squares) in the anterior gray matter; segmented hippocampoal commisure (green) and corresponding reference ROI (orange squares) in the posterior gray matter. (C) Comparison of relative susceptibility in the corpus collasum and (D) in the hippocampal commissure demonstrate a loss of susceptibility contrast in the shiverer mice.

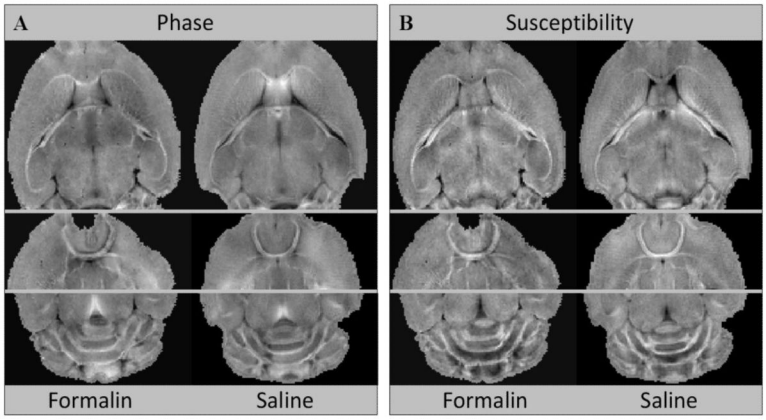

Figure 4.

Comparison of phase and susceptibility maps between brains perfused with formalin and saline from a group of control mice.[R2.4] (A) Three representative phase maps have similar gray-white matter contrast between brains perfused with formalin and saline. (B) The corresponding susceptibility maps also demonstrate similar contrast. Statistical analysis with t-test did not reveal statistically significant differences between the susceptibility values in the white matter between these two types of perfusion procedures.

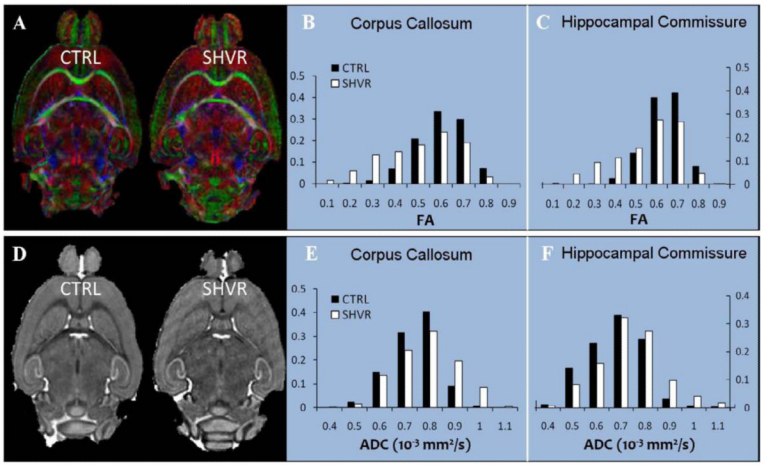

Figure 5.

Intact fiber tracts in the shiverer mice with slightly decreased diffusion anisotropy and increased ADC. (A) A representative slice of color-coded FA map in the control mouse and in the shiverer mouse. The color coding scheme is: red representing rostrocaudal direction, green representing left-right direction and blue representing dorsoventral direction. The color-coded FA maps demonstrate identical fiber orientations in the shiverer as in the control. (B) Comparison of the histograms of FA in the corpus callosum and (C) in the hippocampal commissure reveal slightly decreased FA in the shiverer mouse. (D) A representative ADC map of the control mouse and the shiverer mouse demonstrate a reduced ADC contrast in the shiverer. (E) Comparison of the histograms of ADC in the corpus callosum and (F) in the hippocampal commissure show increased ADC in the white matter of shiverer mice.

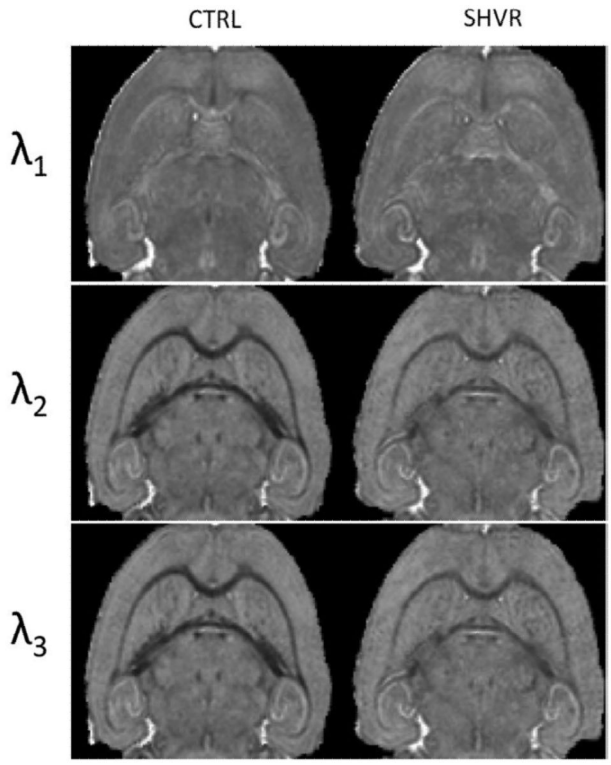

Figure 6.
Comparison of the three eigenvalues of diffusion tensor between the control and the shiverer mouse. The largest eigenvalue (λ1), i.e. the axial diffusivity, remains unchanged. The two smaller eigenvalues (λ2 and λ3), i.e. the radial diffusivity of the white matter, increases in the shiverer mouse, resulting a reduction in tissue contrast. The most significant reduction appears in the smallest eigenvalue (λ3).

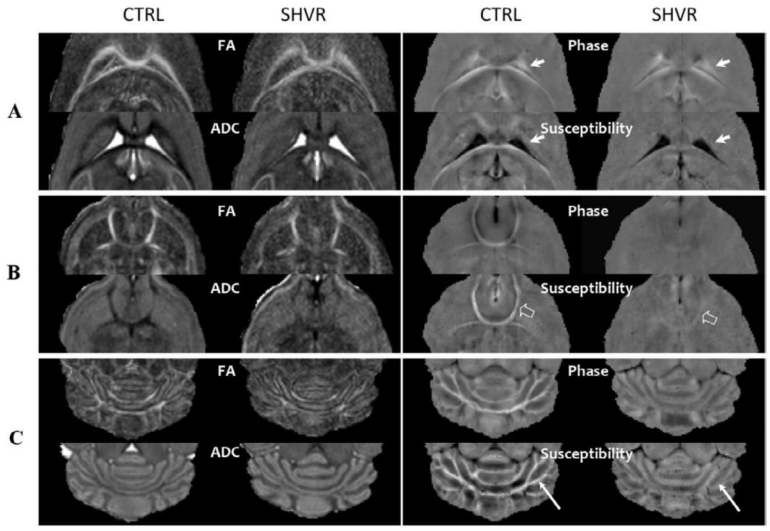

Figure 7.

Diffusion and susceptibility contrast in three selected areas: (A) around the ventricles, (B) in the anterior commissure and (C) the cerebellum. In general, the shiverer mouse exhibits reduced FA and ADC contrast while showing a near absence of susceptibility contrast. In areas near the ventricles (A), the phase map appears bright due to the non-localized nature of phase distribution. However, the quantitative susceptibility map recovers a clear delineation of the tissue-CSF boundary (solid arrows) and reveals an absence of susceptibility contrast between gray and white matter in the shiverer mouse. Interestingly, in the anterior commissure (B), there is a small residual susceptibility contrast in the shiverer mouse (open arrows). In the cerebellum (C), the susceptibility map shows the finest delineation of fiber pathways and the most obvious change in gray and white matter contrast.

Table 1

FA, ADC, Frequency and Susceptibility of Brain Regions in the Control and the Shiverer Mice.

		Gray matter	Corpus callosum	Hippocampal commissure	Anterior commissure	Hippocampus	CSF
FA	CTRL	0.20±0.07	0.61±0.11	0.64±0.09	0.55±0.23	0.43±0.16	0.18±0.10
	SHVR	0.19±0.04	0.51±0.16	0.55±0.15	0.54±0.10	0.40±0.07	0.17±0.11
ADC (10^{-3} mm^2/s)	CTRL	0.93±0.07	0.74±0.09	0.68±0.11	0.77±0.11	0.80±0.10	2.08±0.35
	SHVR	1.03±0.05	0.79±0.15	0.74±0.16	0.98±0.05	0.98±0.06	1.91±0.25
Frequency (Hz)	CTRL	0.49±0.83	−1.95±1.59	−3.27±2.17	−2.21±1.61	−1.22±1.45	0.51±2.14
	SHVR	0.20±0.67	0.34±0.84	0.22±1.17	0.19±0.96	0.23±0.67	−1.19±2.29
χ (10^{-2} ppm)	CTRL	−0.19±0.71	−1.32±1.39	−2.89±1.75	−1.33±1.53	−1.31±1.33	4.90±1.33
	SHVR	−0.23±0.52	0.04±0.61	−0.46±0.79	−0.09±0.65	0.01±0.69	4.34±1.02

(Note: n = 3. The shaded region shows the relative frequency and susceptibility using adjacent gray matter as references.)